arXiv:1701.03601v1 [astro-ph.GA] 13 Jan 2017

Abstract. Closure quantities measured by very long baseline interferometry (VLBI) observations are independent of instrumental and propagation instabilities and antenna gain factors, but are sensitive to source structure. A new method is proposed to calculate a structure index based on the median values of closure quantities rather than the brightness distribution of a source. The results are comparable to structure indices based on imaging observations at other epochs and demonstrate the flexibility of deriving structure indices from exactly the same observations as used for geodetic analysis and without imaging analysis. A three-component model for the structure of source 3C371 is developed by model-fitting closure phases. It provides a real case of tracing how the structure effect identified by closure phases in the same observations as the delay observables affects the geodetic analysis, and investigating which geodetic parameters are corrupted to what extent by the structure effect. Using the resulting structure correction based on the three-component model of source 3C371, two solutions, with and without correcting the structure effect, are made. With corrections, the overall rms of this source is reduced by 1 ps, and the impacts of the structure effect introduced by this single source are up to 1.4 mm on station positions and up to 4.4 microarcseconds on Earth orientation parameters. This study is considered as a starting point for handling the source structure effect on geodetic VLBI from geodetic sessions themselves.

Key words. source structure effect, structure index, VLBI, CONT14, quasars: individual (3C371)

Journal of Geodesy manuscript No.
(will be inserted by the editor)

The impacts of source structure on geodetic parameters demonstrated by the radio source 3C371

Ming H. Xu[1,2], Robert Heinkelmann[2], James M. Anderson[2], Julian Mora-Diaz[2], Maria Karbon[2], Harald Schuh[2,3], and Guang L. Wang[1]

[1] Key Laboratory of Planetary Sciences, Shanghai Astronomical Observatory, Chinese Academy of Sciences, 200030 Shanghai, China
[2] Helmholtz Centre Potsdam, GFZ German Research Centre for Geosciences, Telegrafenberg 14473 Potsdam, Germany
[3] Institute of Geodesy and Geoinformation Science, Technische Universität Berlin, Straβe des 17. Juni 135, 10623, Berlin, Germany

Received: date / Revised version: date

1 Introduction

It is well known from astrophysical studies of imaging that structures of geodetic radio sources are generally asymmetric, time-dependent, and frequency-dependent (e.g., Charlot, 1990a; Ojha et al., 2004, 2005; Piner, 2007; Lister et al., 2009; Charlot, 2010; Fomalont et al., 2011; Lister et al., 2013). The effects of source structures in geodetic very long baseline interferometry (VLBI) have been studied for decades (e.g., Campbell, Schuh & Zeppenfeld, 1988; Charlot, Lestrade & Boucher, 1988; Tang & Rönnäng, 1988; Ulvestad, 1988; Charlot, 1990b; Fey et al., 1996; Tornatore & Charlot, 2007; Shabala et al., 2015; Plank et al., 2016), and, for instance, by studying a series of ten Research and Development VLBI (RDV) sessions, Sovers et al. (2002) concluded that the structure effects contributed 8 ps – 30 ps WRMS residual delay, and were the three major contributors along with the instrumental and tropospheric delays in geodetic VLBI. However, this effect is still ignored as noise in routine geodetic VLBI data analysis so far.

In order to reach the future goals of VGOS (Petrachenko et al., 2009), including 1 mm position accuracy, delay errors from individual sources should also be below approximately 1 mm / c $\sim$ 3 ps, implying that for a typical baseline length of 8000 km for geodetic VLBI observations, the astrometric positions of sources must be accurate to about 25 microarcseconds (μas). The motions and brightness fluctuations of the radio components of the set of regularly observed geodetic quasars are not known well, but worst-case limits can be estimated from studies of other active galactic nuclei source samples. Using the largest high-cadence study of flat-spectrum radio quasars (MOJAVE; Lister et al., 2009), the most common jet speed is 200 μas yr^{-1}, with a maximum jet speed of 2500 μas yr^{-1}, while Fomalont et al. (2011) demonstrated that the jet speed of the geodetic source $0556 + 238$ is about 100 μas yr^{-1}. Such motions would require source structure to typically be redetermined 8 times per year. Alternatively, brightness fluctuations, such as flares in the jet core regions, can also affect the effective astrometric position of sources. Numerous long-term (many years) single-dish monitoring programs show that the rise times to double the total flux densities of sources can be as small as a few months or even a few weeks (see, for example, Aller et al., 1985; Lister et al., 2009; Fuhrmann et al., 2014; Park & Trippe, 2014; Max-Moerbeck, 2016). For a simple structure model of two approximately-equal-brightness components separated by 500 μas with one component undergoing a flare, an astrometric centroid shift of 25 μas results from just a 10 % change in the total brightness.

Clearly, source structure changes must be monitored on timescales far shorter than a year in order to meet the future VGOS goals, and we cannot expect that source structure can be handled merely by selecting sources in VLBI observations based on structure indices that were in many cases obtained from single-epoch observations and separated in time from the geodetic observations by more than a decade. Instead, geodetic VLBI should be able to determine source structure properties from the same observations that are being used to determine geodetic information. Therefore, we propose a method that uses geodetic observations to derive structure indices and study the impacts of structure effects on those same observations. We use an individual source in this paper as a demonstration case; in practice all sources with suitable observations can be analyzed using this method.

2 Closure quantities

It is difficult to use group delay, fringe phase, and observed amplitude to study structures of radio sources owing to instabilities introduced by the atmosphere, independent local oscillators, and varying antenna gains at each site. However, VLBI observations are baseline dependent, and for an interferometer array with more than two stations there are redundancies allowing the formation of closure quantities that are independent of atmospheric effects, clock fluctuations, and any station-based errors.

2.1 Closure delay

We defined closure delay as the sum of the delays around a closed triangle of baselines. Closure delay is a direct and im-

Send offprint requests to:

portant criterion of how much the source structure affects delay observables. It can also be used to determine the measurement noise in geodetic VLBI observables and thus indicate the precision level of delay observables. For a detailed discussion about closure delay, please refer to Xu et al. (2016).

2.2 Closure phase

Closure phase has been used by the astrophysical community to make images of radio sources for decades (Rogers et al., 1974; Pearson & Readhead, 1984, 1988). It is well know that phase delays in VLBI observations are more accurate than group delays, but due to the unresolved ambiguity issue, phase in fact has not been used in geodetic VLBI. Closure phase actually circumvents the ambiguity issue.

2.3 Closure amplitude

Amplitude is generally not calibrated in geodetic VLBI observations, but closure amplitude, independent of the gain of each individual station, is a good observable for the study of source structure. With four stations, a, b, c, and d, it is possible to form combinations of amplitudes that are independent of the antenna's gain factors by using

$$A_{\mathrm{abcd}} = \frac{A_{\mathrm{ab}} A_{\mathrm{cd}}}{A_{\mathrm{ac}} A_{\mathrm{bd}}}, \tag{1}$$

where, for instance, A_{ab} is the observed amplitude on baseline ab. These combinations are called closure amplitude (Readhead et al., 1980). If all six interferometer baselines formed by the four stations are correlated in one scan, three closure amplitudes with different values can be obtained, for example A_{abcd}, A_{abdc}, and A_{adcb}, only two of which are independent. For a comprehensive discusion about closure phase and closure amplitude, please refer to Pearson & Readhead (1984) and Thompson, Moran & Swenson (2007) and the references therein.

2.4 Calculations and data

The interpretation of closure quantities is very challenging, as, unlike the visibility, the sky brightness distribution cannot be obtained from them by a simple Fourier transform relationship. Moreover, knowledge of both the absolute strength and the absolute position of the source is lost in these closure quantities. However, closure quantities have the advantage of showing the magnitudes of source structure effects without the need for calibration or imaging. Source structure effects in geodetic VLBI data analysis have merely been considered in terms of a structure index, so that point-like sources can be selected and extended sources can be avoided in scheduling of VLBI observations. However, for the 1 mm accuracy goal of VGOS, such an approach is unlikely to be sufficient as there are not enough sources with low structure indices ($<$3) to cover the sky uniformly. For most geodetic sources, the structure indices are single epoch and thus might not represent the magnitudes of structure effects in observations after several years. Therefore, it should be more effective and illuminating to determine the magnitudes of structure effects based on closure quantities from geodetic observations themselves.

To demonstrate this, we use the data from CONT14[1] observations (Nothnagel, 2015) at X band. CONT14, as a campaign of continuous VLBI observations conducted by the International VLBI Service for Geodesy and Astrometry (IVS) over 15 days with 17 globally distributed stations, was intended to acquire state-of-the-art VLBI data with the highest accuracy that the then existing VLBI system was capable of. Since only 71 radio sources were observed in this campaign, one can expect that most of these radio sources have enough observations with good uv coverages to get meaningful statistical information from closure quantities.

The specific equations that were used for the calculations of closure quantities from geodetic VLBI observations are shown in Appendix A. Closure quantities were calculated based on these equations. Next, the median and the rms values of the magnitudes of closure delays, closure phases, and closure amplitude logarithms were determined for each source. Due to the sensitivity of rms value to outliers with large magnitudes, rms values were derived in an iterative way: closure quantities with magnitudes 5 times larger than the rms were identified as outliers until no outliers remained. For most radio sources, only a few percent of the closure quantities were excluded in this procedure. The statistics for the 65 radio sources that have more than 30 closure relations in CONT14 observations are presented in Table 1.

3 Structure index

Structure index (Fey & Charlot, 1997, 2000) plays an important role in geodetic/astrometric VLBI as an indicator of the magnitude of the structure effect for each source: (1) extended sources can be avoided and compact sources can be selected in VLBI observations; (2) one of the criteria for selecting defining sources in ICRF2 is that they had structure indices smaller than 3 (Fey et al., 2015); (3) sources with high astrometric quality can be selected as candidate sources for aligning optical and radio catalogs (e.g. Bourda et al., 2008, 2011; Le Bail et al., 2016). Structure index can be calculated from closure delays based on observations if the thresholds for closure delays $\tau^{\mathrm{th}}_{\mathrm{closure}}$ are related to the thresholds for calculated structure corrections in delay observables $\tau^{\mathrm{th}}_{\mathrm{delay}}$ that were used by Fey & Charlot (1997) to calculate structure index. The relation between these two thresholds is,

$$\tau^{\mathrm{th}}_{\mathrm{closure}} = \sqrt{3}\sqrt{\tau^2_{\mathrm{noise}} + \left(\tau^{\mathrm{th}}_{\mathrm{delay}}\right)^2}, \tag{2}$$

where τ_{noise} is the median value of measurement noises. The rms of closure delays for 0727-115, which has minimal source structure and shows no closure structure with baseline orientation (see, Xu et al., 2016), was 8 ps, which suggests that the measurement noise of individual group delays is below 4.8 ps (8 ps/$\sqrt{3}$). According to the relative relationship between rms and median values, the median value of the measurement noise was set to be 2.8 ps. Furthermore, note that

[1] http://ivscc.gsfc.nasa.gov/program/cont14/

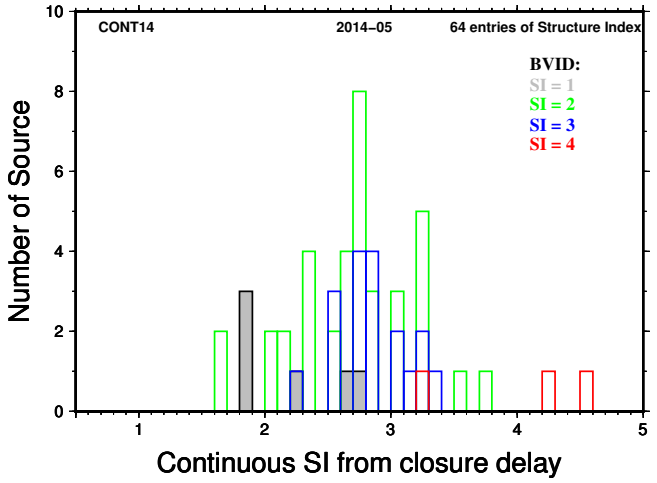

Fig. 1. The distribution of continuous structure indices of 64 radio sources. Each color represents one group of structure index in the BVID and each group is shown independently.

changing this value to around 5 ps does not change classifying the structure indices between 2 and 3 or 3 and 4 — it only affects distinguishing a structure index of 1 from 2. In order to facilitate comparison to the Bordeaux VLBI image database[2] (BVID), which unfortunately only contains integer structure indices near in time to the CONT14 sessions, we define an integer closure delay structure index as follows. Using the same thresholds of structure delays for classifying structure groups in Fey & Charlot (1997), and assuming $\tau_{\rm noise}$ = 2.8 ps, the structure index (SI) can also be calculated from the median value of closure delays by,

$$SI = \begin{cases} 1, & \text{if } 0 \text{ ps} \le |\tau_{\rm closure}|^{\rm med} < 7.1 \text{ ps}, \\ 2, & \text{if } 7.1 \text{ ps} \le |\tau_{\rm closure}|^{\rm med} < 18.0 \text{ ps}, \\ 3, & \text{if } 18.0 \text{ ps} \le |\tau_{\rm closure}|^{\rm med} < 52.2 \text{ ps}, \\ 4, & \text{if } 52.2 \text{ ps} \le |\tau_{\rm closure}|^{\rm med} < \infty. \end{cases} \quad (3)$$

We further define a continuous closure structure index that closely approximates equation 3 of an integer structure index as:

$$SI \equiv \ln \frac{|\tau_{\rm closure}|^{\rm med}}{1 \text{ ps}}. \quad (4)$$

This equation is for closure delays, and a complete set of equations for the three kinds of closure quantities are presented in Appendix B.

Integer structure indices for the 65 radio sources were derived according to equation 3 and shown in column 11 of Table 1 labeled as closure delay (CD1), while the continuous structure indices calculated from equation 4 based on closure delays are shown in the last column referred to as CD2. For comparison, the most recent structure indices at X band from the BVID, which unfortunately are integer, are presented in column 10. The BVID structure indices are in the time range of April 2004 to July 2013 with an average of 2011, about three years earlier than CONT14 observations. There is one source, 0637−752, that is not found in the BVID and it was identified to have structure index of 3 at X band from closure delays. Structure indices of 14 radio sources were found to have increased, either from 1 to 2 (3 sources) or 2 to 3 (11 sources); those of 13 radio sources have decreased, from 3 to 2 (10 sources), 2 to 1 (2 sources), or 4 to 3 (1 source); while the remaining 37 radio sources have the same structure indices. The most frequent changes between our identified structure indices and those from the BVID are the transitions between structure indices of 2 and 3. The distribution of continuous structure indices are presented in Fig. 1. The rms of the differences between the continuous structure indices from closure delays and those from the BVID is 0.61.

Median absolute values of the three closure quantities as a function of the longest projected baseline length in the triangle or in the quadrangle are shown for 54 radio sources in Fig. 2. The natural logarithms of closure amplitudes for source 0738+313 deviate considerably from zero even for very small quadrangles, which means that it has a strong structure with a quite large spatial scale. Almost all other radio sources have a common pattern in their plots that median absolute values of closure quantities start with small values and increase when the projected baseline lengths become larger. Variations of the three closure quantities agree well with each other.

These plots graphically demonstrate the median absolute closure quantities from Table 1 that were used to calculate the structure indices, and also illustrate that the amount of source structure effects depends on baseline length. For example, source 0642+449 shows very little structure effect in the three closure quantities for short baselines but has very significant effects when the projected baselines are larger than about 8000 km. This shows that it is strongly resolved on small spatial scales, which may be a recent development since it was selected as a defining source in ICRF2 and has a structure index of 2 in BVID. In this case, rms values of closure quantities represent the magnitude of structure effect much better than median values. On the other hand, the median values for source 0016+731 are very small and have a flat pattern, and only slightly increase when the projected baseline lengths are larger than 11000 km; it is classified as having structure index of 1 based on closure delays. It is worth noting that the median values of the three closure quantities in general are much smaller than the rms values. So called "good" sources with a structure index of 2 still tend to have quite significant rms closure delays. Also, the structure indices of "good" and "extended" sources depend strongly on the date of observation, with 36% of "good" and "extended" sources changing structure index between the BVID and the CONT14 sessions.

4 Investigating impacts of source structure effect

The results presented in Tab. 1 suggest that the source 3C371 is a good candidate for the preliminary study of impacts of structure effect because: (1) it has tens of thousand closure quantities in CONT14 and a structure index of 3; (2)the median values of its closure quantities are large even when the projected baseline lengths are small so that many observables are affected by structure; and (3) compared to the struc-

[2] http://www.obs.u-bordeaux1.fr/BVID/

Table 1. Statistics of closure quantities and structure indices for 65 radio sources in CONT14 observations. Column 2 is the total number of triangles and column 7 is the total number of quadrangles for each source formed based on these observations.

SOURCE	$N_{\rm tri}$	$\lvert\tau_{\rm closure}\rvert^{\rm med}$ (ps)	$\tau^{\rm rms}_{\rm closure}$ (ps)	$\lvert\phi_{\rm closure}\rvert^{\rm med}$ (deg.)	$\phi^{\rm rms}_{\rm closure}$ (deg.)	$N_{\rm qua}$	$\lvert\ln A_{\rm closure}\rvert^{\rm med}$	$(\ln A_{\rm closure})^{\rm rms}$	structure index BVID	CD1	CD2
0014+813	15141	42.7	64.9	18.8	65.9	69062	0.548	0.961	2	3	3.8
0016+731	23307	5.7	10.0	3.3	6.1	114970	0.097	0.164	2	1	1.7
0017+200	3380	15.3	33.1	6.8	16.2	12585	0.209	0.360	2	2	2.7
0059+581	33755	6.5	12.8	3.4	7.7	167895	0.143	0.240	1	1	1.9
0106+013	3279	16.3	36.5	9.4	19.0	9668	0.251	0.591	1	2	2.8
0119+115	980	17.9	31.1	5.1	8.6	1555	0.206	0.469	2	2	2.9
0212+735	18631	28.2	69.5	25.1	54.7	92255	0.578	1.079	4	3	3.3
0229+131	3136	31.7	83.8	17.2	58.9	10937	0.418	0.806	2	3	3.5
0322+222	640	23.7	47.5	13.7	25.0	2075	0.262	0.377	2	3	3.2
0332−403	2676	19.2	31.4	9.4	17.4	4361	0.172	0.317	2	3	3.0
0420−014	10479	11.0	20.0	7.1	13.4	40717	0.186	0.374	2	2	2.4
0454−234	5681	13.1	21.3	4.0	7.0	13608	0.115	0.168	2	2	2.6
0528+134	620	19.1	34.1	10.0	17.9	951	0.171	0.239	3	3	2.9
0529+483	15027	24.0	44.2	9.4	15.9	65080	0.190	0.317	2	3	3.2
0537−441	3780	13.6	21.7	6.6	11.0	6412	0.141	0.230	2	2	2.6
0607−157	7432	26.6	87.2	10.8	47.0	19547	0.646	1.102	3	3	3.3
0637−752	1174	31.5	86.3	15.8	58.4	1230	0.342	1.031	-	3	3.4
0642+449	22154	21.1	119.0	11.4	48.4	98559	0.462	0.824	2	3	3.0
0657+172	10946	16.4	30.4	8.6	18.4	51460	0.187	0.315	2	2	2.8
0716+714	26767	9.3	16.2	3.7	6.2	132691	0.077	0.130	1	2	2.2
0727−115	11224	6.3	8.2	1.8	2.9	35874	0.121	0.221	1	1	1.8
0738+313	13994	100.6	232.3	36.4	75.1	67137	0.749	1.153	4	4	4.6
0748+126	16018	12.7	21.8	8.1	13.2	72260	0.169	0.284	3	2	2.5
0749+540	5339	17.2	30.0	11.1	20.7	20256	0.212	0.380	3	2	2.8
0814+425	8470	15.2	26.1	8.1	12.1	36226	0.126	0.189	2	2	2.7
0827+243	3045	13.7	25.0	4.9	8.1	10953	0.131	0.266	1	2	2.6
0919−260	434	25.8	45.7	11.2	15.8	489	0.497	0.553	3	3	3.3
0955+476	7032	11.1	18.6	4.1	7.3	27993	0.085	0.142	2	2	2.4
1044+719	2303	5.4	9.6	3.1	6.5	8551	0.102	0.152	2	1	1.7
1053+815	862	11.5	19.0	5.4	8.4	2297	0.088	0.133	2	2	2.4
1104−445	298	17.8	27.7	11.4	17.9	198	0.248	0.365	3	2	2.9
1124−186	5214	17.5	28.6	7.6	13.2	13743	0.184	0.363	2	2	2.9
1156+295	1754	20.3	40.5	8.7	23.5	6471	0.179	0.265	3	3	3.0
1308+326	316	10.8	16.9	4.8	8.3	574	0.136	0.188	2	2	2.4
1406−076	282	16.0	27.4	7.4	12.9	645	0.451	0.234	3	2	2.8
1417+385	2433	14.0	25.1	3.8	7.2	9204	0.083	0.129	2	2	2.6
1424−418	5482	7.0	11.0	2.6	5.4	10295	0.115	0.177	1	1	1.9
1448+762	1486	12.6	25.3	6.1	11.8	4897	0.291	0.584	3	2	2.5
1519−273	3341	16.6	28.3	6.1	10.6	6716	0.124	0.185	2	2	2.8
1611+343	15235	12.8	21.0	6.5	11.2	69563	0.176	0.296	3	2	2.5
1639−062	5593	19.3	32.8	6.2	11.2	16341	0.152	0.273	2	3	3.0
1739+522	31157	29.6	57.8	14.0	33.2	150648	0.339	0.584	3	3	3.4
1741−038	6184	7.4	13.3	4.9	8.4	18738	0.134	0.255	2	2	2.0
1751+288	10501	7.9	14.8	3.9	8.0	47261	0.096	0.164	2	2	2.1
1806+456	3458	11.7	24.9	4.2	8.7	12480	0.138	0.278	2	2	2.5
1846+322	14942	28.0	63.2	7.4	33.0	66839	0.309	0.551	2	3	3.3
1921−293	1225	7.7	12.8	2.1	3.7	1686	0.178	0.509	2	2	2.0
1954−388	1496	17.7	28.2	9.9	14.9	2214	0.160	0.295	3	2	2.9
2000+472	13718	17.2	33.8	4.9	10.3	61370	0.231	0.413	3	2	2.8
2052−474	369	25.2	40.6	6.9	10.2	286	0.261	0.350	2	3	3.2
2059+034	556	23.9	33.8	8.5	19.9	2008	0.357	0.450	2	3	3.2
2113+293	281	21.6	31.8	7.8	12.0	667	0.256	0.351	3	3	3.1
2121+053	168	18.3	27.2	14.3	20.1	352	0.254	0.347	3	3	2.9
2145+067	4631	15.9	30.0	13.5	39.0	14173	0.304	0.687	2	2	2.8
2201+315	84	14.2	22.5	5.1	7.4	86	0.239	0.324	2	2	2.7
2209+236	4018	18.8	46.2	7.3	25.2	16516	0.321	0.574	2	3	2.9
2214+350	3377	16.5	29.7	5.6	9.7	12589	0.111	0.170	2	2	2.8
2227−088	1732	12.6	23.5	7.0	11.4	5597	0.145	0.267	2	2	2.5
2234+282	293	9.8	15.6	3.9	6.4	526	0.148	0.146	3	2	2.3
2255−282	531	13.8	23.5	4.6	11.2	525	0.139	0.152	2	2	2.6
2309+454	752	8.3	14.1	3.9	8.3	2491	0.091	0.142	2	2	2.1
2355−106	1078	16.1	27.3	6.0	12.2	3257	0.150	0.295	2	2	2.8
3C309.1	350	63.5	98.3	17.6	27.0	388	0.481	0.756	4	4	4.2
3C371	27133	20.4	46.6	18.0	27.9	136392	0.307	0.709	3	3	3.0
4C39.25	9861	17.0	41.9	13.0	33.2	39947	0.522	0.866	3	2	2.8

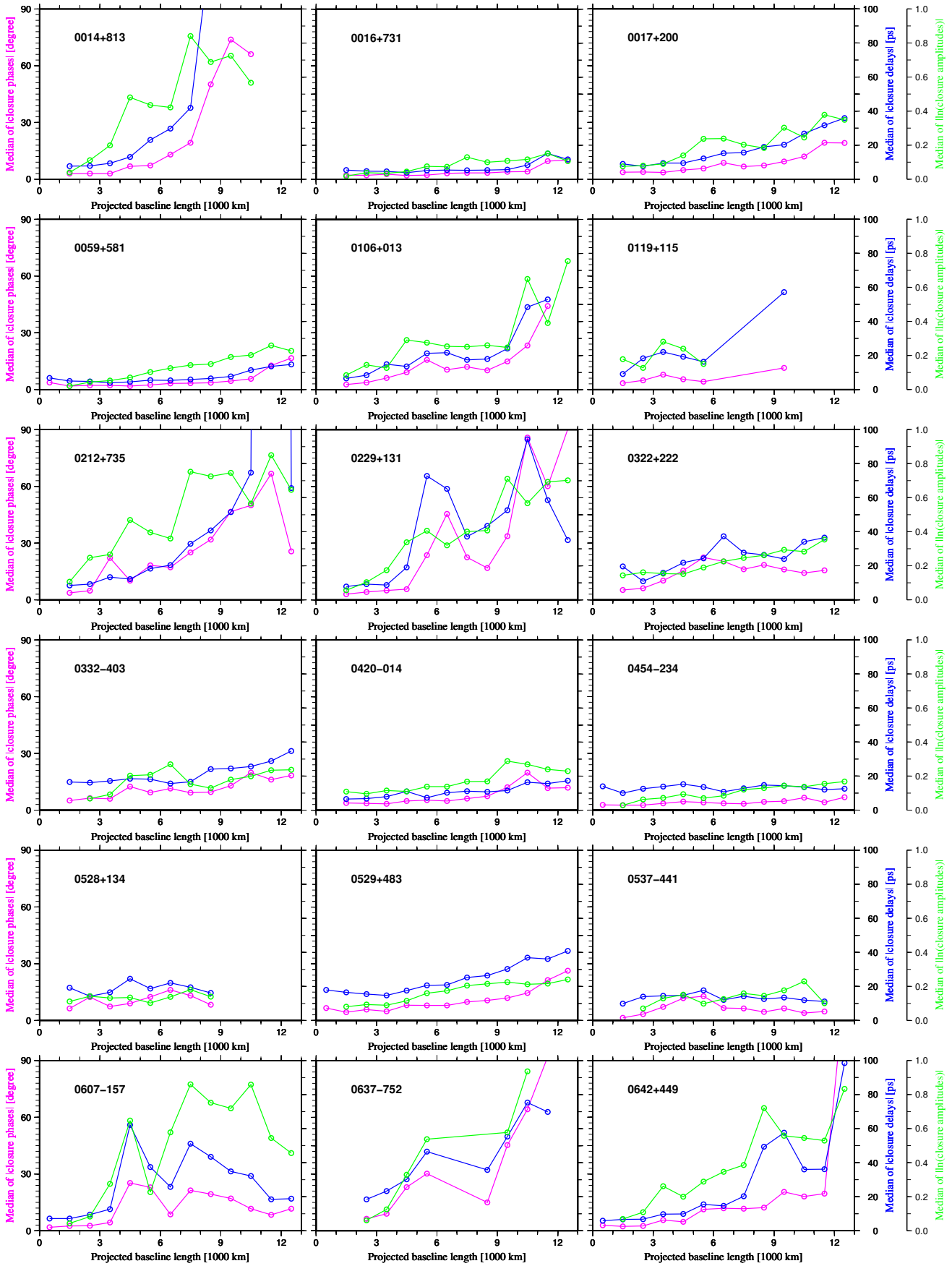

Fig. 2. Variations of the median absolute values of closure delays, closure phases, and natural logarithms of closure amplitudes with respect to the longest baseline length in the triangle or the quadrangle for the 54 most observed radio sources in CONT14.

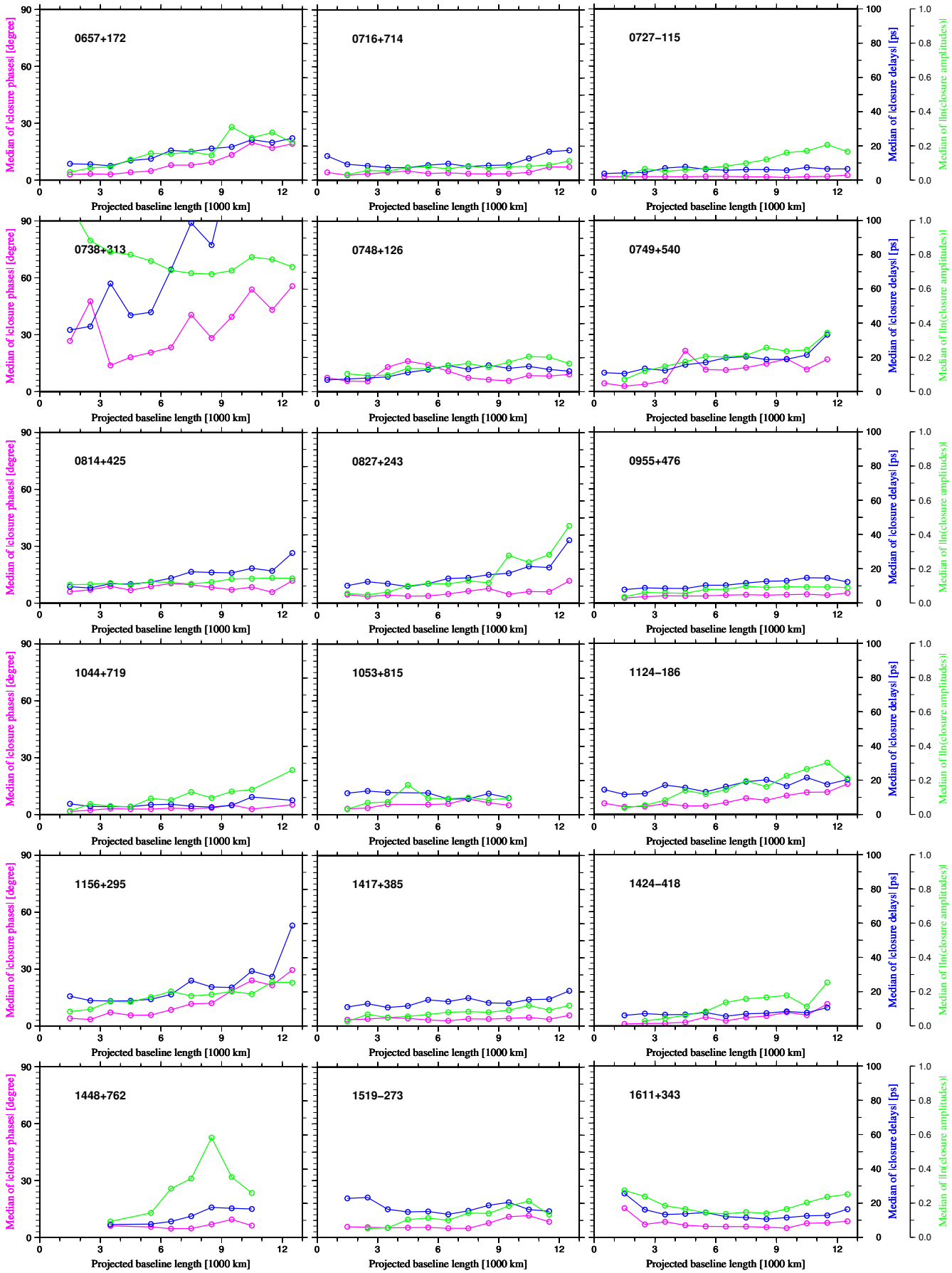

Fig. 2. - Continued

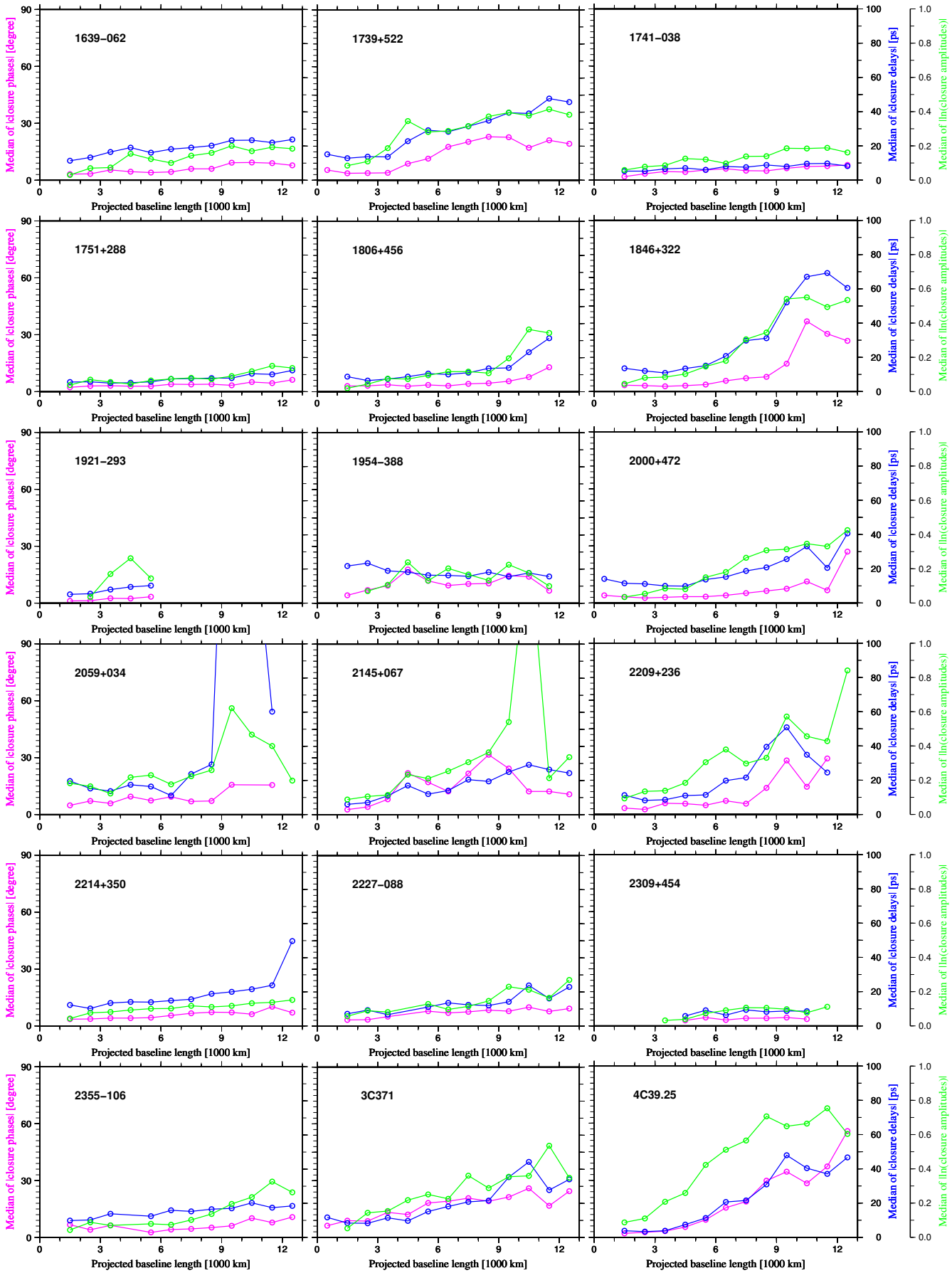

Fig. 2. - Continued

ture effects of some extended sources, such as 0014+813 and 0738+313, the structure effects of 3C371 are not so strong such that observables with significant structure effects would be excluded as outliers during VLBI data analysis. From Fig. 2, we also notice that 3C371 is a good representative of the radio sources in CONT14 in the sense of the magnitude of source structure effects.

4.1 Structure model for 3C371

The structure of source 3C371 was assumed to have multiple point components and was determined by model-fitting of closure phases directly instead of the traditional Fourier imaging. The method of forward modeling was developed to determine the multi-component structure: (1) closure phases of small triangles with longest baseline lengths shorter than a certain value, such as 2000 km, are used to determine the relative position and the flux-density ratio of two components based on the model of structure phase in Charlot (1990b); (2) closure phases of triangles with larger baseline lengths are gradually added and used to test the obtained multi-component model by the previous step until a significant mismatch between modeled closure phases and observed closure phases occurs; (3) another component is proposed and fitted from closure phases and then the second step is repeated; and (4) fitting continues until the closure phases of triangles with the longest baseline length are exploited. In the whole procedure, the identified components are kept and only one new component will be proposed to add in at one time.

If one does not have any a priori information about the structure of a source, different a priori values for the two-component model may need to be tested. In general, however, the changing pattern of closure phases of triangles with the same three stations over 24-hours of GMST should give useful insight for that.

Based on this method, a three-component model was determined for the source 3C371. The result is presented in Table 2 and shows that this source is extended in one direction with a position angle of about 260°. From publicly available maps of 3C371 in Feb. 2014 and Sep. 2015[3], we find a good agreement in the position offset and direction of extended structure between our modeling and imaging results. To make a direct modeling to imaging comparison, we have imaged the CONT14 sessions' visibility data for 3C371, shown in Fig. 3. Our image shows a core with a one-sided jet extending about 6 mas from the core along a position angle of about 260°. No significant structure is visible farther than 6 mas from the core, in contrast to the VLBA imaging results mentioned directly above. However, the IVS CONT14 observations have longer baselines, more observations with long baselines, and fewer short-VLBI baselines, than observations provided by the VLBA, so it is not surprising that our imaging results show no emission at large separations from the core, where the emission is expected to be more extended and therefore resolved-out. The details of imaging based on geodetic VLBI sessions and a detailed comparison between the images from geodetic sessions and VLBA sessions will be presented in our future publication (Anderson et al., in prep.).

[3] http://astrogeo.org/vlbi_images/

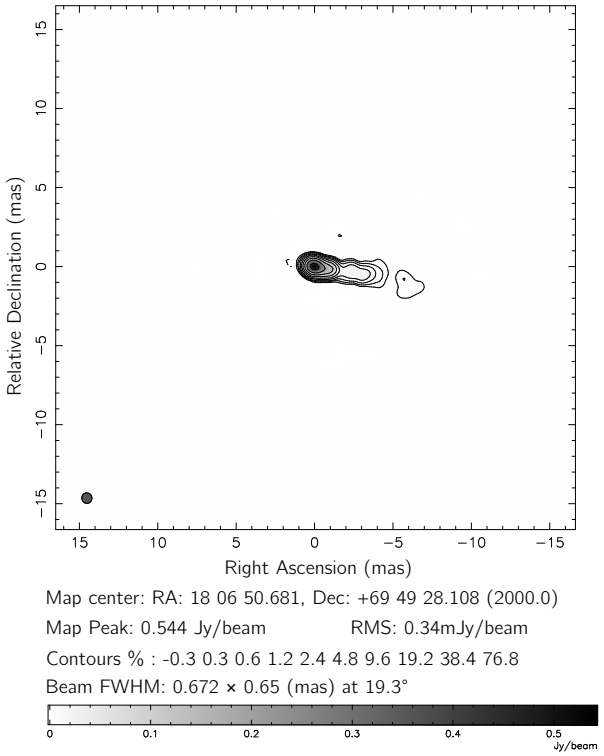
Relative Declination (mas)
Right Ascension (mas)
Map center: RA: 18 06 50.681, Dec: +69 49 28.108 (2000.0)
Map Peak: 0.544 Jy/beam
RMS: 0.34mJy/beam
Contours % : -0.3 0.3 0.6 1.2 2.4 4.8 9.6 19.2 38.4 76.8
Beam FWHM: 0.672 × 0.65 (mas) at 19.3°
Jy/beam

Fig. 3. The image of 3C371 based on the visibility data from CONT14 sessions using natural weighting. The extended direction from our proposed method using closure phases agrees well with the imaging result.

Fig. 4 shows observed closure phases in magenta dots, modeled closure phases from the proposed analysis in blue dots, and closure phases from imaging results in green dots for two triangles as a function of GMST. The rms of closure phases was reduced from 27.9° to 12.5° using the three-component model. As we can see, the results from imaging have only a slightly better agreement with the observed closure phases and delays, and the model based on closure quantities does give results close to what full imaging gives.

The three-component model then was used to calculate the structure corrections for delay observables at X band and the effect at S band was ignored. By applying this structure model to group delays, the rms of closure delays of 3C371 was reduced from 46.6 ps to 36.4 ps. Fig. 5 shows observed closure delays, modeled closure delays from the three-component model, and closure phases from imaging for the same two triangles in Fig. 4. Modeled closure delays generally have the same pattern as that in observations, however, the scatter in the variations of closure delays is much larger than that in closure phases, and the structure delays from the structure models cannot exactly follow the variations in observed closure delays. The improvement in closure phases after modeling the source structure effects is 55 %, while that in closure delays is only 22 %. This shows the expected result that the observed phases are more accurate than the observed delays and provide better modeling constraints.

The theoretical delay software CALC11 was modified to be capable of correcting the structure effect. The theoretical delays for all observations in CONT14 were recalculated to

Table 2. Structure model of 3C371 determined by model-fitting from closure phases. The first component with the peak intensity was set to be the reference point. The flux-density ratios k and the relative offsets r are with respect to the reference point. PA is the position angle of the vector of the component and the reference point, measured in the sky counterclockwise with respect to the north.

Component	k	r (mas)	PA (deg.)
1	1	0	0
2	0.302 ± 0.007	0.504 ± 0.052	257.0 ± 3.2
3	0.235 ± 0.010	1.001 ± 0.058	261.3 ± 4.5

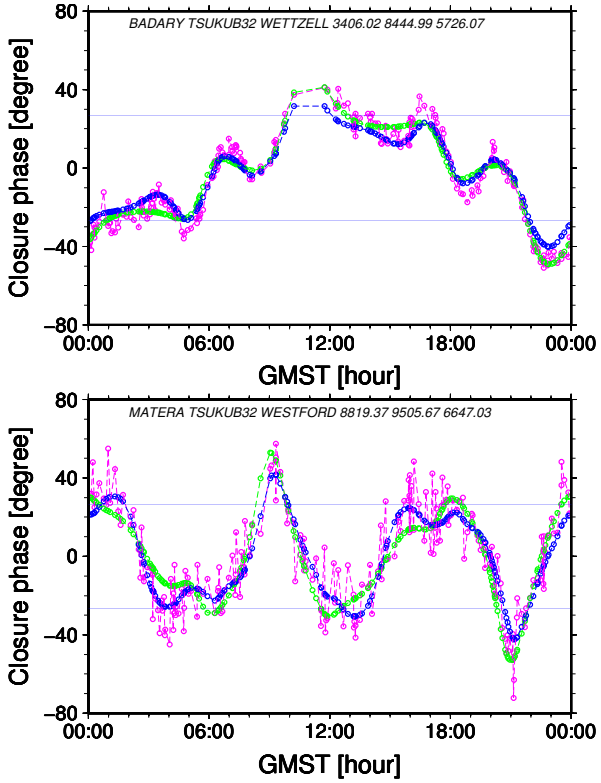

Fig. 4. Comparison between closure phases from the three-component model (blue), the imaging result (green) and the observations (magenta) for two closure triangles.

generate new databases. Two solutions were then made based on the new databases and the original databases.

4.2 Impacts of source structure effect

A detailed comparison of results obtained from the two sets of databases was made to investigate the impacts of structure effect introduced by one single radio source, 3C371. In total there are about 254 000 observations. The overall rms and chi-square for the solution of the original IVS databases were 26.65 ps and 0.832, respectively, while those for the new databases are 26.61 ps and 0.830. Comparisons of residual rms for 3C371 over 15 sessions are presented in Table 3. About 12 000 observables of 3C371 were included in the data analysis. The overall rms for this source was reduced from 26 ps to 25 ps, and the chi-square was decreased from 0.863 to 0.835.

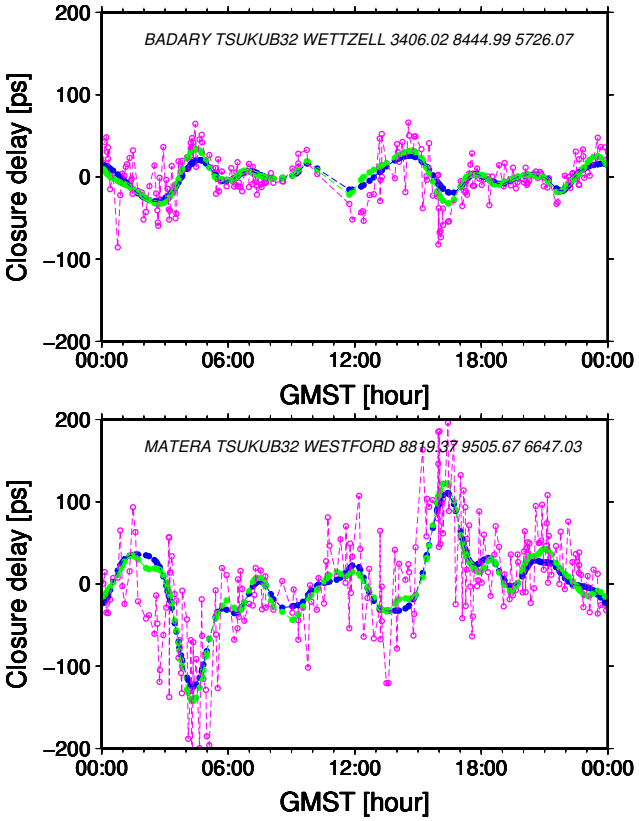

Fig. 5. Comparison between closure delays from the three-component model (blue), the imaging result (green) and the observations (magenta) for two closure triangles.

Table 3. Comparison of residual delay rms for source 3C371. The second column shows the numbers of used observables in the data analysis and the numbers of usable observables in the databases. Two solutions are based on exactly the same ensemble of observables.

SESSION	No. of obs. used/usable	rms from new databases (ps)	rms from IVS databases (ps)
14MAY06XA	1141/1161	25.4	26.1
14MAY07XA	868/878	24.7	25.5
14MAY08XA	950/964	25.3	26.3
14MAY09XA	627/650	24.8	26.1
14MAY10XA	812/827	26.0	26.5
14MAY11XA	678/684	25.5	26.4
14MAY12XA	660/681	28.2	29.0
14MAY13XA	704/712	26.3	27.3
14MAY14XA	827/843	27.3	28.2
14MAY15XA	709/720	24.8	25.5
14MAY16XA	787/827	24.7	25.5
14MAY17XA	682/702	23.1	24.2
14MAY18XA	764/796	23.2	24.1
14MAY19XA	549/556	24.4	25.4
14MAY20XA	861/902	22.1	22.8

The baseline repeatability for most of baselines was improved in a range up to 0.04 mm. The comparison for the baselines related to YARRA12M is shown in Table 4 as an example.

Table 4. Comparision of the rms of time-series of baseline lengths over 15 days for all baselines of YARRA12M. (Unit: mm)

BASELINE	rms of baseline length new databases	IVS databases
KATH12M-YARRA12M	3.12	3.12
HOBART12-YARRA12M	3.55	3.55
HOBART26-YARRA12M	3.56	3.55
WARK12M-YARRA12M	3.82	3.82
TSUKUB32-YARRA12M	5.57	5.57
HART15M-YARRA12M	8.61	8.62
BADARY-YARRA12M	3.54	3.55
KOKEE-YARRA12M	4.19	4.20
YARRA12M-ZELENCHK	3.64	3.66
MATERA-YARRA12M	3.90	3.94
WETTZELL-YARRA12M	3.90	3.91
NYALES20-YARRA12M	4.01	4.03
ONSALA60-YARRA12M	3.94	3.96
YARRA12M-YEBES40M	4.01	4.02

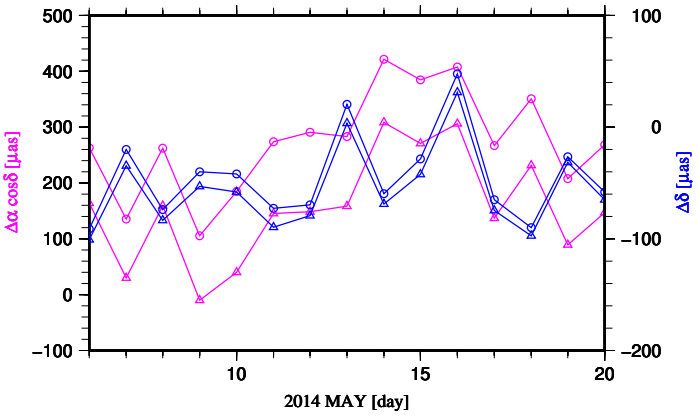

Fig. 6. Comparison of estimated position corrections of source 3C371 to its ICRF2 position with its structure effect corrected or not. The circles represent the time series from the original IVS databases, while the triangles represent that from the new databases with the aim of correcting the structure effect.

The differences between results of polar motion and nutation/precession parameters from the two datasets over 15 days were at the level of microarcseconds with a maximum of 4.4 microarcseconds, and those for UT1 were below 0.1 microsecond. The coordinates of stations WESTFORD and ZELENCHK have the biggest differences, about 1.4 mm in the U direction, while the rest of the stations have agreement in three coordinates at the level of 0.2 mm.

The direction of source 3C371 was estimated as a global parameter to be ($18^{\rm h}\ 06^{\rm m}\ 50\overset{\rm s}{.}680\,675$, $+69^\circ\ 49'\ 28\overset{''}{.}108\,484$) from the IVS databases and to be ($18^{\rm h}\ 06^{\rm m}\ 50\overset{\rm s}{.}680\,664$, $+69^\circ\ 49'\ 28\overset{''}{.}108\,472$) from the new databases. The difference is 165 microarcseconds in right ascension and 12 microarcseconds in declination. This difference should be due to the reference point used for the calculation of the structure effect, which is the peak intensity of the brightness distribution in the study. Another pair of solutions, in which the position of source 3C371 was fit as session-wise parameter, were made to get the time series of source's position. The results are presented in Fig. 6. The main difference is a constant offset in right ascension, which can be removed by choosing an appropriate reference point for calculating the structure delay corrections. The variation in the source's position remains at the level of a few hundred microarcseconds, which suggests that the modeled structure effect for this source in bandwidth synthesis and ionospheric effect free delay observables does not perform as well as that for phases. The differences in the positions of the remaining sources are about 3 microarcseconds or below that for global sources and up to 10 microarcseconds for session-wise sources.

5 Discussion and conclusion

The source structure effects in CONT14 observations were studied in terms of closure delays, closure phases, and closure amplitudes. A method of deriving structure index based on closure quantities was proposed, and structure indices for 65 radio sources with at least 30 closure triangles were obtained according to this method. This result is comparable to structure indices from the BVID and the closure quantities in principle capture important information about source structure. The equations of closure delay structure indices are derived from exactly the same thresholds of structure delays as that were used by Fey & Charlot (1997). This allows our closure delay structure indices to hold the same meaning of structure index as its original definition. There are, however, two main differences between the structure indices from these two methods: (1) because our closure delay structure indices are derived from actual observables and the BVID structure indices are from theoretical predictions of only structure delay based on images, our closure delay structure indices have to take the measurement noise into account, while this is not the case for the BVID structure indices; (2) our closure delay structure indices are determined from the actual (u, v) coordinates sampled in a session, whereas the structure indices of Fey & Charlot (1997) are calculated from a grid sampling all possible ground-based VLBI (u, v) coordinates. Further investigations, based on the same datasets of the structure indices from the BVID, of our method and of the influence of the different observing networks are definitely needed. Therefore, the structure indices for geodetic sources can be regularly updated without making images, for instance, from all the VLBA and VLBA plus global VLBI stations sessions, IVS terrestrial reference frame sessions, and even from IVS R1 and R4 sessions for a fraction of radio sources. Structure index is conservatively defined by the median absolute value of structure effect corrections, although the median values of closure quantities are in general significantly smaller than their rms values. The structure effects in geodetic VLBI may have been underestimated. According to our study the rms values are better than the median values in terms of demonstrating the magnitude of structure effect.

Source 3C371 was selected as a starting point for the study of impacts of structure effect on geodetic VLBI data analysis. A three-component model of the structure of 3C371, derived by model-fitting from closure phases, was used to correct its structure delay. The structure model derived from phases does not fit with the delay observables as well as the phase observables. The results show the impacts of structure effect by this *individual* source on EOPs is up to about 4.4 microarcseconds and on station's position in some cases are beyond 1

mm. The estimated source position is strongly dependent on the reference point of the structure model.

Even though this preliminary study of the structure effects for an individual source can be limited to summarizing the significance of correcting for the structure effect, there are at least three conclusions that can be made. First, although source structure effects may be averaged out to some extent when solving for geodetic parameters, in particularly for an individual source in this study, they are crucial for determining the position of each individual source. Without correcting the source structure effects, a source position determined from geodetic observations does not have a clear reference point, neither the location of the peak intensity nor the center of the brightness, because the estimated source position strongly depends on the specific baseline geometries of observations. But with the effects corrected, we can explicitly say where the determined source position is located with respect to the source structure. For instance, we can say that the reported source position in the case of 3C371 after correcting these effects is the location of the peak intensity identified from our method. If we use a map of a source to correct the effects, then we can provide the location of the reference point for the estimated source position in the map. Since the difference between the positions with and without correcting structure effects is at the level of sub-milliarcseconds, and larger differences can be expected for some sources, this is very important for high-accuracy relative astrometry. In addition, with the possibility of identifying the cores of sources, we can realize a more stable celestial reference frame. Second, the impact on station position in some cases is already beyond 1 mm. Third, the residual rms for source 3C371 was reduced by 1 ps. This is significant, even though there is still room for the improvement of the structure model. From our study, an improvement in geodetic VLBI data analysis of, at least, the picosecond level can be expected after a complete consideration of structure effects.

This study demonstrates the preliminary results of structure effect. Only 10% of radio sources have a structure index of 1 in CONT14. Sources with a structure index of 2, the majority in geodetic VLBI observations, actually have rms closure delay at the level of 30 ps, which significantly contribute to the total residual rms of VLBI data analysis. A rigorous and consistent method of handling the source structure is to correct the structure phases, based on the brightness distribution obtained from that epoch, for the raw phases in all channels used in the recording system during the post-processing procedure and then re-determine multi-band group delays and ionosphere corrections.

Acknowledgements. We acknowledge the International VLBI Service for Geodesy and Astrometry (IVS) and all of its components for their efforts in observing, correlating, and providing the VLBI data used in this study. We thank the three anonymous referees for thoughtful readings and valuable comments, and Leonid Petrov (Astrogeo Center, USA) for the helpful discussions about this work. This research has made use of material from the Bordeaux VLBI Image Database (BVID). This work was done while MH worked as a guest scientist at GFZ, Germany, and was supported by the National Natural Science Foundation of China (grant No. 11473057 and 11303077).

References

Aller HD, Aller MF, Latimer GE, Hodge PE (1985) Spectra and linear polarizations of extragalactic variable sources at centimeter wavelengths, ApJS, 59:513

Bourda G, Charlot P, Campion JFL (2008) Astrometric suitability of optically-bright ICRF sources for the alignment with the future Gaia celestial reference frame, A&A 490:403

Bourda G, Collioud A, Charlot P, Porcas P, Garrington S (2011) VLBI observations of optically-bright extragalactic radio sources for the alignment of the radio frame with the future Gaia frame. II. Imaging candidate sources, A&A 526:102

Campbell J, Schuh H, Zeppenfeld G (1988) On the Computation of Group Delay Corrections Caused by Radio Source Structure, in: Reid MJ (eds) The Impact of VLBI on Astrophysics and Geophysics, p. 427

Charlot P (1990a) Fourteen extragalactic radio sources mapped at 2.3 and 8.4 GHz with a 24-hour Crustal Dynamics Program VLBI experiment, A&A 229:51

Charlot P (1990b) Radio-source structure in astrometric and geodetic very long baseline interferometry, AJ 99:1309

Charlot P, Boboltz DA, Fey AL, Fomalont EB, Geldzahler BJ, Gordon D, Jacobs CS, Lanyi GE, Ma C, Naudet CJ, Romney JD, Sovers OJ, Zhang LD (2010) The Celestial Reference Frame at 24 and 43 GHz. II. Imaging, AJ 139:1713

Charlot P, Lestrade JF, Boucher C (1988) 3C 273 and DA 193 Mapped with Crustal Dynamics VLBI Data, in: Reid MJ (eds) The Impact of VLBI on Astrophysics and Geophysics, p. 33

Fey AL, Clegg AW, Fomalont EB (1996) VLBA Observations of Radio Reference Frame Sources. I, ApJS 105:299

Fey AL, Charlot P (1997) VLBA Observations of Radio Reference Frame Sources. II. Astrometric Suitability Based on Observed Structure, ApJS 111:95

Fey AL, Charlot P (2000) VLBA Observations of Radio Reference Frame Sources. III. Astrometric Suitability of an Additional 225 Sources, ApJS 128:17

Fey AL, Gordon D, Jacobs CS, Ma C, Gaume RA, Arias EF, Bianco G, Boboltz DA, Böckmann S, Bolotin S, Charlot P, Collioud A, Engelhardt G, Gipson J, Gontier A-M, Heinkelmann R, Kurdubov S, Lambert SB, Lytvyn S, MacMillan DS, Malkin Z, Nothnagel A, Ojha R, Skurikhina E, Sokolova JR, Souchay J, Sovers OJ, Tesmer V, Titov OA, Wang G, Zharov VE (2015) The Second Realization of the International Celestial Reference Frame by Very Long Baseline Interferometry. AJ 150:58

Fomalont E, Johnston K, Fey AL, Boboltz D, Oyama T, Honma M (2011) The Position/Structure Stability of Four ICRF2 Sources, AJ 141:91

Fuhrmann L, Larsson S, Chiang J, Angelakis E, Zensus JA, Nestoras I, Krichbaum TP, Ungerechts H, Sievers A, Pavlidou V, Readhead ACS, Max-Moerbeck, Pearson TJ (2014) Fermi bright blazars, MNRAS 441:1899

Le Bail K, Gipson JM, Gordon D, MacMillan DS, Behrend D, Thomas CC, Bolotin S, Himwich W E, Baver KD, Corey BE, Titus M, Bourda G, Charlot P, Collioud A (2016) IVS Observation of ICRF2-Gaia Transfer Sources, AJ 151:79

Lister ML, Cohen MH, Homan DC, Kadler M, Kellermann KI, Kovalev YY, Ros E, Savolainen T, Zensus JA (2009) MOJAVE: Monitoring of Jets in Active Galactic Nuclei with VLBA Experiments. VI. Kinematics Analysis of a Complete Sample of Blazar Jets, AJ 138:1874

Lister ML, Aller MF, Aller HD, Homan DC, Kellermann KI, Kovalev YY, Pushkarev AB, Richards JL, Ros E, Savolainen T (2013) MOJAVE. X. Parsec-scale Jet Orientation Variations and Superluminal Motion in Active Galactic Nuclei, AJ 146:120

Max-Moerbeck W (2016) AGN variability in the radio band, in Proceedings of a conference: Active Galactic Nuclei: what's in a name? DOI: 10.5281/zenodo.60378

Nothnagel A (2015) The IVS data input to ITRF2014, International VLBI Service for Geodesy and Astrometry, DOI: http://doi.org/10.5880/GFZ.1.1.2015.002

Ojha R, Fey AL, Johnston KJ, Jauncey DL, Reynolds JE, Tzioumis AK, Quick JFH, Nicolson GD, Ellingsen SP, Dodson RG, McCulloch PM (2004) VLBI Observations of Southern Hemisphere ICRF Sources. I. AJ 127:3609

Ojha R, Fey AL, Charlot P, Jauncey DL, Johnston KJ, Reynolds JE, Tzioumis AK, Quick JFH, Nicolson GD, Ellingsen SP, McCulloch PM, Koyama Y (2005) VLBI Observations of Southern Hemisphere ICRF Sources. II. Astrometric Suitability Based on Intrinsic Structure. AJ 130:2529

Pearson TJ, Readhead ACS (1984) Image formation by self-calibration in radio astronomy, ARAA 22:97

Pearson TJ, Readhead ACS (1988) The milliarcsecond structure of a complete sample of radio source. II. first-epoch maps at 5 GHz, ApJ 328:114

Park JH, Trippe S (2014) Radio Variability and Random Walk Noise Properties of Four Blazars, ApJ 785:76

Petrachenko, B., Niell, A., Behrend, D., et al. (2009) Design Aspects of the VLBI2010 System, NASA/TM-2009-214180, ftp://ivscc.gsfc.nasa.gov/pub/misc/V2C/TM-2009-214180.pdf

Piner BG, Mahmud M, Fey AL, Gospodinova K (2007) Relativistic Jets in the Radio Reference Frame Image Database. I. Apparent Speeds from the First 5 Years of Data, AJ 133:2357

Plank L, Shabala SS, McCallum JN, Krásná H, Petrachenko B, Rastorgueva-Foi E, Lovell J (2016) On the estimation of a celestial reference frame in the presence of source structure, MNRAS 455:343

Readhead ACS, Walker RC, Pearson TJ, Cohen MH (1980) Mapping radio sources with uncalibrated visibility data, Nature 285:137

Rogers AEE, Hinteregger HF, Whitney AR, Counselman CC, Shapiro II, Wittels JJ, Klemperer WK, Warnock WW, Clark TA, Hutton LK (1974) The structure of radio sources 3C 273B and 3C 84 deduced from the closure phase and visiblity amplitudes observed with three-element interferometers, ApJ 193:293

Shabala SS, McCallum JN, Plank L, Böhm J (2015) Simulating the effects of quasar structure on parameters from geodetic VLBI, J Geod 89:873

Sovers OJ, Charlot P, Fey AL, Gordon D (2002) Structure Corrections in Modeling VLBI Delays for RDV Data, In: Vandenberg NR, BaverKD (eds) Proceedings of InternationalVLBI service for geodesy and astrometry 2002 general meeting, Tsukuba, NASA/CP-2002-210002, p. 243

Tang G, Rönnäng B (1988) Monitoring of Extragalactic Radio Sources via Geodetic VLBI Observations, in: Reid MJ (eds) The Impact of VLBI on Astrophysics and Geophysics, p. 431

Thompson AR, Moran JM, Swenson GM (2007) Interferometry and Synthesis in Radio Astronomy, John Wiley & Sons

Tornatore V, Charlot P (2007) The impact of radio source structure on European geodetic VLBI measurements, J Geod 81:469

Ulvestad JS, Moran JM (1988) Effects of source structure on astrometry and geodesy, in: Reid MJ (eds) The Impact of VLBI on Astrophysics and Geophysics, p. 429.

Xu MH, Heinkelmann R, Anderson JM, Mora-Diaz J, Schuh H, Wang GL (2016) The source structure of 0642+449 detected from the CONT14 observations, AJ 152:151

A Specification for the calculations of closure quantities

To the accuracy of the second order in delay, the closure delay $\tau_{\rm abc}(t)$ at reference epoch t for three stations a, b, and c, is calculated from geodetic VLBI observations[4] by

$$\begin{aligned}\tau_{\rm abc}(t) =&\tau_{\rm ab}(t) + \tau_{\rm bc}(t) - \tau_{\rm ac}(t)\\ &+ [\dot{\tau}_{\rm bc}(t)\cdot \tau'_{\rm ab}(t) + \frac{1}{2}\ddot{\tau}_{\rm bc}(t)\cdot \tau'_{\rm ab}(t)^2],\end{aligned} \tag{5}$$

where, for instance, $\tau_{\rm ab}$ is the group delay observable from station a to station b, and $\tau_{\rm bc}$ is the group delay observable from station b to station c, for the same wavefront received by three stations. A prime on a delay symbol indicates that the term refers only to the geometric delay without dependence on station clock offset, and a superposed dot and double superposed dots denote differentiation with respect to time once and twice, respectively. The definition and model of closure delay was discussed in detail by Xu et al. (2016). By convention in geodetic VLBI measurements, the time tag of a VLBI observable is referred to the epoch when the wavefront passes the first station in the baseline. In order to have the three delay observables in the closure refer to the the same wavefront, there are the corrections in the brackets of equation 5 to the group delay for the second baseline in the triangle.

Similar to closure delay, closure phase can be calculated from geodetic VLBI observations[5] by using

$$\begin{aligned}\phi_{\rm abc}(t) =&\phi_{\rm ab}(t) + \phi_{\rm bc}(t) - \phi_{\rm ac}(t)\\ &+ [\dot{\tau}_{\rm bc}(t)\cdot \tau'_{\rm ab}(t) + \frac{1}{2}\ddot{\tau}_{\rm bc}(t)\cdot \tau'_{\rm ab}(t)^2]\cdot 2\pi\nu,\end{aligned} \tag{6}$$

where, for instance, $\phi_{\rm ab}$ is fringe phase observable on baseline ab, and ν is the reference frequency. We should be aware that τ, $\dot{\tau}$, and $\ddot{\tau}$ in equation 6 are phase delay and the derivatives of phase delay, and are different from the group delay terms in equation 5.

For closure amplitude, in order to have closure amplitude quantities be zero for point-like sources, like closure delay and closure phase, we calculate the absolute value of natural logarithm of the closure amplitude by

$$C_{\rm amp} = |\ln(A_{\rm abcd})|. \tag{7}$$

B Equations for determing structure index from closure quantities

Continuous structure index from closure quantities is defined as follows:

$$SI_{\rm clo\text{-}dela} \equiv \ln \frac{|\tau_{\rm closure}|^{\rm med}}{1\ {\rm ps}}, \tag{8}$$

$$SI_{\rm clo\text{-}phas} \equiv 0.77 \ln \frac{|\phi_{\rm closure}|^{\rm med}}{1\ {\rm deg}} + 1.26, \text{ and} \tag{9}$$

[4] For astronomical observations that reference all observables for a scan to the same wavefront, the model of closure delay has the simpler form $\tau_{\rm abc}(t) = \tau_{\rm ab}(t) + \tau_{\rm bc}(t) - \tau_{\rm ac}(t)$.

[5] For astronomical data, $\phi_{\rm abc}(t) = \phi_{\rm ab}(t) + \phi_{\rm bc}(t) - \phi_{\rm ac}(t)$.

$$SI_{\text{clo-amp}} \equiv 2.67\,|\ln A_{\text{closure}}|^{\text{med}} + 2.14. \quad (10)$$

The form of equation 8 was selected to match the integer steps of equation 3, not to match the continuous structure index of Fey & Charlot (1997). A least square fit was performed based on the CONT14 observations to determine the coefficiences in equations 9 and 10, by matching the closure phase and closure amplitude structure indices as well as possible to the closure delay structure indices. Generalized, exact forms of these equations for their applications to other observations need to be investigated carefully.